

Two classes of radio flares in the blazar PKS 0420–014

J. F. Zhou^{1,2}, X. Y. Hong^{1,2}, D. R. Jiang^{1,2}, and T. Venturi³

ABSTRACT

The two 5GHz VLBI (Very Long Baseline Interferometry) observations (1996 June and 1997 November) presented in this paper, combined with several former VLBI observations at 8.4GHz and 5GHz, suggest that the radio flares of the blazar PKS 0420–014 can be divided into two classes according to their geometric origins in 5 or 8.4GHz VLBI maps and the properties of light curves. One class of flares, which we call *core flares*, originate from the core. Core flares have large lags between the light curves at different frequencies, and will probably lead to the ejection of new jet components. The other class of flares, which we call *jet flares*, come from jet components. Jet flares vary simultaneously at different wavelengths, and may due to the Doppler boosting effect of rotating knots moving along a helical jet. The radio flare in 1991, accompanied by a simultaneous gamma-ray flare, was identified as a core flare.

Subject headings: radiation mechanisms: non-thermal— BL Lacertae objects: individual (PKS 0420–014)— gamma rays: bursts—radio continuum: general— techniques: interferometric

1. INTRODUCTION

The blazar PKS 0420–014 ($z=0.915$) is active and strongly variable at all wavelengths. It is a ROSAT source (Brinkmann, Siebert, and Boller 1994) and has been identified as an EGRET gamma-ray source (Fichtel et al. 1994).

The total flux density of PKS 0420–014 has been monitored extensively at many wavelengths. The routine monitoring at 4.8, 8.0, and 14.5GHz was carried out by the 26m paraboloid in the University of Michigan (Aller et al. 1985). The millimeter and submillimeter observations at 22, 37, 90, 150, 230, 270, and 375GHz were taken at the 15-m James Clerk Maxwell Telescope (JCMT), SEST (Swedish-ESO submillimetre Telescope), the IRAM 30m telescope (Steppe et al. 1988, 1992, 1993) and MRRS (Metsähovi Radio Research Station) (Teräsanta et al. 1992). Simultaneous optical and gamma-ray flare was detected in 1992 (Wagner et al. 1995).

The blazar PKS 0420–014 has been observed with VLBI at 43GHz, 8.4GHz, 5GHz and 2.3GHz since 1986. Five images at 8.4GHz and the results from model fitting are given in Wagner et al. (1995) and Fey, Clegg, and Fomalont (1996). Images at 5 GHz are presented in Wehrle et al. (1992), Shen et al. (1997) and Hong et al. (1999), who observed the source in 1986, 1992 and 1995 respectively. These observations show that the jet components move along a bending trajectory. Superluminal proper motion was found in this source (Wagner et al. 1995; Shen et al. 1997; Hong et al. 1999).

Some properties of the radio flares were successfully explained by a model incorporating an adiabatically expanding shocked region (Hughes, Aller, and Aller 1989). Stevens et al. (1995) investigated the spectral evolution of the radio flares occurred in 1991 and 1992 in PKS 0420-014.

In this paper we present two 5GHz VLBI observations, carried out in 1996 June and 1997 November. An analysis of our data and former VLBI results, combined with the study of the total flux density variations, led us to identify the location of the emitting regions of these flares, which we classify according to the properties of

¹Shanghai Astronomical Observatory, No. 80, Nandan Road, Shanghai 200030, China

²National Astronomical Observatories, CAS, China

³Istituto di Radioastronomia del CNR, Via Gobetti 101, I-40129 Bologna, Italy

their light curves. Throughout this paper, the values $H_0 = 100h \text{ km s}^{-1} \text{ Mpc}^{-1}$ and $q_0 = 0.5$ will be used.

2. CLASSIFICATION OF THE RADIO FLARES

The long term light curves at 4.8, 8.0, and 14.5GHz are shown in Figure 1. In order to compare the flare flux density, we subtracted the quiescent core flux density at each frequency, assuming a flat quiescent core spectrum. The quiescent core flux density, about 1.2 Jy, was estimated from 8.4GHz VLBI observation at epoch 1994.52, when the source was in its lowest state. From the data plotted in Figure 1 we can identify six strong flares (represented by 1, 2, 3, 4, 5, and 6), which occurred in 1983, 1985, 1990, 1992, 1995, and 1998. Some minor flares may also exist, but they are not very significant at these three frequencies.

We classified the flares according to the time lags of the maximums at the various frequencies. Flare 2 and 5 are characterized by large lags between the peaks of light curves at different frequencies. We use polynomials to fit the un-averaged flux data and then determine the peaks of the light curves (see Table 1). For flare 2, the lags Δt between 14.5 and 8.0 GHz and between 8.0 and 4.8 GHz are $\Delta t_{8.0}^{14.5} = 0.62 \pm 0.10 \text{ yr}$ and $\Delta t_{4.8}^{8.0} = 0.52 \pm 0.10 \text{ yr}$ respectively. The corresponding lags for flare 5 are $\Delta t_{8.0}^{14.5} = 0.36 \pm 0.10 \text{ yr}$ and $\Delta t_{4.8}^{8.0} = 0.53 \pm 0.10 \text{ yr}$ respectively. We named these as *core flares*, or *Class I flares* ($\Delta t_{8.0}^{14.5} > 0.2 \text{ yr}$). The remaining strong flares show no or small lags and can be grouped together. The prototype of this class is flare 4. Its light curves reach their peak simultaneously at epoch 1992.6 ± 0.1 . We named these *jet flares* or *Class II flares* ($\Delta t_{8.0}^{14.5} < 0.2 \text{ yr}$).

This classification still holds when we add 37 GHz and 90 GHz data (see Figure 1). Large time lags exist between the millimeter and centimeter light curves of flare 5, while flare 4 peaks simultaneously in the whole range of frequencies from 4.8 GHz to 90 GHz. A new remarkable feature is a strong millimeter flare occurred at the end of 1991 (represented by G in Figure 1). The corresponding centimeter flare was much weaker. Since it shows lags between high and low frequencies, we classify it as a Class I flare. We will discuss it in

detail in section 4.

3. VLBI OBSERVATIONS

Our two 5GHz VLBI observations were carried out on 1996 June 17, and on 1997 November 07 with EVN (European VLBI Network). Eight telescopes took part in the 1996 observations, i.e. Shanghai, Crimea, Noto, Hartbeesthoek (affiliated), Urumqi, Onsala, WSRT, and Torun. The nine telescopes participating in the 1997 observations are Effelsberg, Jodrell Bank, Medicina, Shanghai, Noto, Hartbeesthoek, Urumqi, WSRT, and Torun. The recording modes were MkIII mode E (bandwidth 14MHz) and MkIII mode B (bandwidth 28MHz) for the 1996 and 1997 epochs respectively. The data were correlated at MPIfR Mk III correlator in Bonn.

A-priori amplitude calibration and fringe-fitting were carried out using the standard routines in the AIPS package. Imaging was done using the DIFMAP difference mapping software (Shepherd, Pearson, and Taylor 1994). The 1996 and 1997 final images are shown in Figure 2. For the map of 1996, the noise is 1.68mJy/beam, the map peak is 1.41Jy/beam, and the FWHM is $1.08 \times 0.85 \text{ (mas)}$ at -85.8° . For the map of 1997, the noise is 1.85mJy/beam, the map peak is 1.37Jy/beam, and the FWHM is $1.17 \times 0.79 \text{ (mas)}$ at -81.4° . In order to carry out the image analysis, we used the program 'modelfit' in DIFMAP to fit the final self-calibrated UV data with gaussian components. The model fitting results are given in Table 2. We estimate that the errors of the parameters are: $\Delta \text{Flux} = \pm 20\%$, $\Delta \text{Radius} = \pm 0.1 \text{ mas}$, $\Delta \text{P.A.} = \pm 5^\circ$, $\Delta \theta = \pm 10\%$, $\Delta \text{Rat.} = \pm 15\%$ and $\Delta \text{p.a.} = \pm 20^\circ$.

It is clear from Figure 2 and Table 2 that the two images differ considerably. The size and flux of the core are very similar in the two epochs. However the position of the first jet component (A) with respect to the core changed from 1.1 mas to 1.3 mas going from 1996 to 1997. Its position angle also changed, and the flux decreased from 0.39 to 0.15 Jy. The result of our model fitting shows that component B is stationary.

In Figure 3 we plotted the relative positions of the jet components with respect to the core from 1990.38 to 1997.85. In this figure positions 1, 2, 3, 4 (Wagner et al. 1995), and 6 (Fey, Clegg, and Fo-

malont 1996) are from 8.4GHz images; positions 5 (Shen et al. 1997), 7 (Hong et al. 1999), 8, and 9 are from 5GHz images. The observing epochs are listed in legend. For each epoch we identified the component closest to the core with component A in our images, and the more distant component with B. From Figure 3, it is clear that component A emerges from the core in the south-west direction. At Radius ~ 1.3 mas and P.A. $\approx -145^\circ$, the jet bends abruptly and turns from south-west to south-east, and then slowly curves to south, which is in agreement with the large scale VLBI map at 18cm (Fey, Clegg, and Fomalont 1996) and VLA (Very Large Array) map at 20cm (Antonucci, and Ulvestad 1985).

The position of component A changes smoothly from 1990.38 to 1995.82, suggesting a proper motion $\mu = 0.12 \pm 0.02$ mas yr $^{-1}$, which corresponds to a liner velocity of $3.1 \pm 0.5h^{-1}c$. This jet component probably emerged from the core at ~ 1985.5 when strong flare 2 visible in Figure 1 began. While the position of A in 1997.85 is in good agreement with this proper motion, its location in 1996.46 is difficult to understand, both because of the large motion from 1995.82 to 1996.46, i.e. $\mu \sim 0.6$ mas yr $^{-1}$ and because of the abrupt change in position angle. It is possible that we mis-identified component A in 1996.46. We also note that the location of component A in 1996.46 is in much better agreement with the location of component B at the epochs labelled 2, 3 and 4.

Another remarkable feature in Figure 3 is the different kinematical behaviour of component A, within 1.3 mas from the core, and component B, beyond this distance. Component B does not appear continuously along the jet path. Gaps where the jet is undetected are clearly visible. This can be easily explained assuming that the jet component (or knot) moves along a helical jet path and rotates around the jet axis. Under this assumption the viewing angle of the jet component changes continuously. When the viewing angle near its minimum value, the corresponding Doppler factor is large and the component is visible; when the viewing angle near its maximum value, the corresponding Doppler factor is small, and the component may disappear.

In order to locate the origin of the radio flares, we add the total VLBI flux density, the core flux density and the flux density of component A of

ten VLBI observations in Figure 1. Both the total VLBI flux density and the core flux density were subtracted by 1.2 Jy of quiescent core flux. As we can see from Figure 1, the Class 1 flares, such as the 1985 one, are dominated by a core flux density increase, while the flux density variations of jet component are much less and can be neglected. On the other hand, Class 2 flares are dominated by jet flares. A typical such flare happened in 1992. Near the peak of this flare, VLBI observation (Shen et al. 1997) showed that the flux of the component A was 1.7 Jy, much greater than the 0.8 Jy core flare flux. The core flare flux density is comparable with the flux of the component A during the intervals between 1990 and 1992 and between 1995 and 1997.

We conclude that PKS 0420–014 is characterized by two different classes of flares, originating in different source regions: Class 1 radio flares originate in the core, while Class 2 flares come from jet components.

4. DISCUSSION

Optical depth is essential to explain the observed phenomena. In VLBI, 'core' actually refers to the optically thick inner jet with flat spectrum, while 'jet' refers to the optically thin outer jet with steep spectrum. As a new flare component generates in the core region, its emission will gradually become optically thin from high frequencies to low frequencies. As a results, we see the time-lagged core flares. The jet flares, however, probably happens in the optically thin jet region.

The classification of radio flares depends on their light curves as well as VLBI results. However, the core size in VLBI maps depends on the observing frequency and resolution. A flare component might be resolved as a jet component in a 43GHz high resolution VLBI map but still in the core in a 5GHz low resolution VLBI map. So, here, we need to point out that core flare happens within the core region based on 5GHz or 8.4GHz VLBI observations, usually with one milliarcsec resolutions.

We propose that jet flares are due to the Doppler boosting effect of knots moving along a helical jet. All the VLBI observations available show that the proper motion of the jet component emerged at 1985.5 is nearly constant. This im-

plies that the variation of the Lorentz factor and of the viewing angle are small. Small variation of Lorentz factor would not cause large variation of flux. However, because the average viewing angle of the jet in PKS 0420–014 is small (about 5.5° Hong et al. (1998)), even a small change in the viewing angle would cause a great change of Doppler factor as well as the flux of jet component (Blandford and Königl 1979). Furthermore, the Doppler factor is independent of the observing wavelength, which can naturally explain the simultaneous jet flares at different wavelengths. The intrinsic variation of the parameters of jet components may also cause flux variation, but cannot fully explain the observed facts.

The flare which took place at the end of 1991 was classified as core flare on the basis of a 5 months lag between the peak at 90GHz and at 14.5GHz. Furthermore, Krichbaum et al. (1994) detected a new jet component in a 43GHz VLBI observation at epoch 1992.40. This component was about 0.2mas (private communication) away from the core, and was probably ejected during the late 1991 flare. However, the core flare in 1991 differs from the other core flares. It was much stronger at millimeter than at centimeter frequencies; its flux density increase was very sharply at the beginning and faded away quickly; last but not least it was accompanied by a simultaneous gamma-ray flare. Thus, more work is needed to study the mechanism of this flare.

We thank an anonymous referee for his/her helpful comments. This research has made use of data from the University of Michigan Radio Astronomy Observatory which is supported by funds from the University of Michigan. Zhou thanks Merja Tornikoski for generously presenting the 37GHz and 90GHz SEST observed flux data of PKS 0420-014. This research has been supported by The Major State Basic Research Development Program and NNSFC no. 19773019.

REFERENCES

- Antonucci, Robert R.J., and Ulvestad, James S. 1985, *ApJ*, 294, 158
- Aller, H.D., Aller, M.F., Latimer, G.E., and Hodge, P.E. 1985, *ApJS*, 59, 513
- Blandford, R.D., and Königl, A., 1979, *ApJ*, 232, 34
- Brinkmann, W., Siebert, J., and Boller, T. 1994, *A&A*, 281, 355
- Fey, A.L., Clegg, A.W., and Fomalont, E.B. 1996, *ApJS*, 105, 299
- Fichtel, C.E., et al. 1994, *ApJS*, 94, 551
- Hong, X.Y., et al. 1998, *Chinese Physics Letters*, Vol. 15, No. 7, 545
- Hong, X.Y., et al. 1999, *A&AS*, 134, 201
- Hughes, P.A., Aller, H.D., and Aller, M.F. 1989, 341, 54
- Krichbaum, T.P., et al. 1994, in *Proc. 2nd EVN/JIVE Symp.*, ed. A.J. Kus, R.T. Schilizzi, K.M. Borkowski, and L.I. Gurvits (Torun Radio Astronomy Observatory Press. Poland), 47
- Shen, Z.-Q., Wan, T.-S., Moran, J.M. et al., 1997, *AJ*, 114, 1999
- Shepherd, M.C., Pearson, T.J., and Taylor, G.B. 1994, *BAAS*, 26, 987
- Steppe, H., et al. 1988, *A&AS*, 75, 317
- Steppe, H., et al. 1992, *A&AS*, 96, 441
- Steppe, H., et al. 1993, *A&AS*, 102, 611
- Stevens, J.A., et al. 1995, *MNRAS*, 275, 1146
- Teräsranta, H., et al. 1992, *A&AS*, 94, 121
- Wagner, S.J., et al. 1995, *A&A*, 298, 688
- Wehrle, A.E., et al. 1992, *ApJ*, 391, 589

This 2-column preprint was prepared with the AAS L^AT_EX macros v5.0.

TABLE 1
EPOCHS OF THE PEAKS OF THE LIGHTCURVES AT DIFFERENT FREQUENCIES.

Freq. (GHz)	1 (yr)	2 (yr)	3 (yr)	4 (yr)	5 (yr)	6 (yr)	G (yr)
4.8	83.54	87.16	90.89	92.54	96.71	x	x
8.0	83.40	86.64	90.67	92.60	96.24	98.59	x
14.5	83.35	86.02	90.61	92.60	95.88	98.52	92.04
37	x	x	x	92.63	x	x	91.76
90	x	x	x	x	95.62	x	91.64

TABLE 2
MODEL FITTING RESULTS.

Epoch	Comp.	Flux (Jy)	Radius (mas)	P.A. (deg)	FWHM (mas)	Rat.	p.a. (deg)
1996.46	Core	1.77	0.0	0.0	0.62	0.63	-20
	A	0.39	1.1	-162	1.56	0.36	-63
	B	0.18	2.6	170	2.40	0.01	84
1997.85	Core	1.84	0.0	0.0	0.66	0.69	28
	A	0.15	1.3	-144	0.91	0.01	81
	B	0.13	2.6	161	2.00	0.01	59

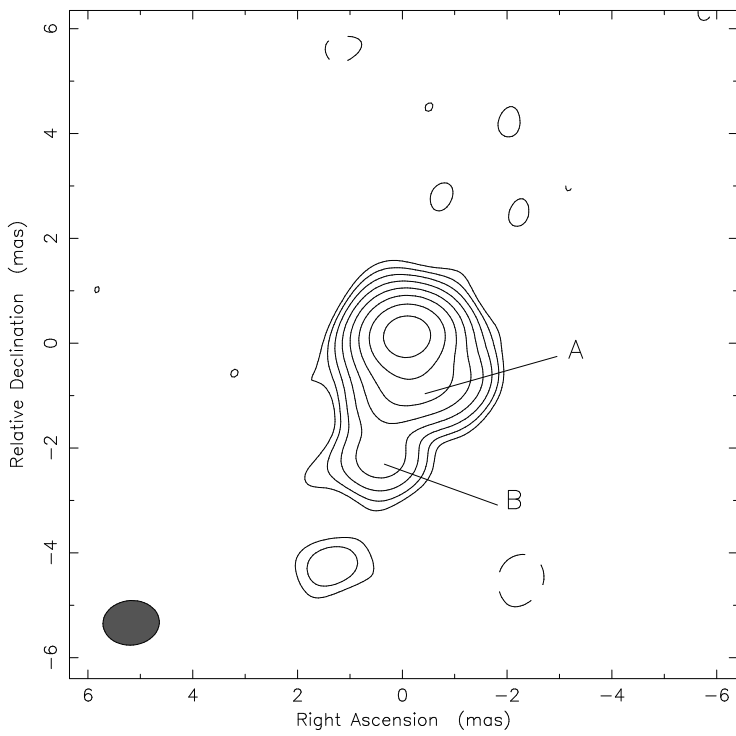
NOTE.—Radius and P.A. refer to the relative orientation w.r.t. the core; FWHM, Rat., and p.a. refer to the average width, axis ratio and orientation of the individual components.

Fig. 1.— Flare flux data of single dish observations and VLBI observations(T represent the total flare flux of VLBI structures; C represent the core flare flux; and F represent the flux of the component A). Light curves were shifted upwards 0Jy for 4.8, 1Jy for 8.0, 3Jy for 14.5, and 7Jy for 37 and 90GHz data.

Fig. 2.— Two CLEAN maps of 0420-014 in 1996(left) and 1997(right). A and B indicate the locations of the first and second jet components. The contours are -0.5 0.5 1 2 4 8 16 32 and 64 percent of map peaks.

Fig. 3.— Relative locations of the jet components
A and B in 0420-014.

Clean map. Array: SRNoEUSWZ
0420-014 at 4.976 GHz 1996 Jun 17



Clean map. Array: ESJLNoEUWZ
0420-014 at 4.974 GHz 1997 Nov 07

